Alveolar macrophage chromatin is modified to orchestrate host response to *Mycobacterium bovis* infection

Thomas Jonathan Hall [1], Douglas Vernimmen [2, *], John Andrew Browne [1], Michael P. Mullen [3], Stephen Vincent Gordon [4, 5], David Evan MacHugh [1, 4, *] and Alan Mark O'Doherty [1]

[1] Animal Genomics Laboratory, UCD School of Agriculture and Food Science, College Dublin, Belfield, Dublin, D04 V1W8, Ireland.

[2] The Roslin Institute, University of Edinburgh, Easter Bush Campus, Midlothian, EH25 9RG, UK.

[3] Bioscience Research Institute, Athlone Institute of Technology, Dublin Road, Athlone, Co. Westmeath, N37 HD68, Ireland.

[4] UCD School of Veterinary Medicine, University College Dublin, Belfield, Dublin, D04 W6F6, Ireland.

[5] UCD Conway Institute of Biomolecular and Biomedical Research, University College Dublin, Belfield, Dublin, D04 V1W8, Ireland.

*** Corresponding authors:**

Douglas Vernimmen douglas.vernimmen@roslin.ed.ac.uk

David E. MacHugh david.machugh@ucd.ie

Keywords

ChIP-seq, chromatin, macrophage, mycobacteria, *Mycobacterium bovis*, tuberculosis

Abstract

Background: Bovine tuberculosis is caused by infection with *Mycobacterium bovis*, which can also cause disease in a range of other mammals, including humans. Alveolar macrophages are the key immune effector cells that first encounter *M. bovis* and how the macrophage epigenome responds to mycobacterial pathogens is currently not well understood.

Results: Here, we have used chromatin immunoprecipitation sequencing (ChIP-seq), RNA-seq and miRNA-seq to examine the effect of *M. bovis* infection on the bovine alveolar macrophage (bAM) epigenome. We show that H3K4me3 is more prevalent, at a genome-wide level, in chromatin from *M. bovis*-infected bAM compared to control non-infected bAM; this was particularly evident at the transcriptional start sites of genes that determine programmed macrophage responses to mycobacterial infection (e.g. M1/M2 macrophage polarisation). This pattern was also supported by the distribution of RNA Polymerase II (PolII) ChIP-seq results, which highlighted significantly increased transcriptional activity at genes demarcated by permissive chromatin. Identification of these genes enabled integration of high-density GWAS data, which revealed genomic regions associated with resilience to infection with *M. bovis* in cattle.

Conclusions: Through integration of these data, we show that bAM transcriptional reprogramming occurs through differential distribution of H3K4me3 and PolII at key immune genes. Furthermore, this subset of genes can be used to prioritise genomic variants from a relevant GWAS data set.

Background

Bovine tuberculosis (bTB) is a chronic infectious disease of livestock, particularly domestic cattle (*Bos taurus* and *Bos indicus*), which causes more than $3 billion in losses to global agriculture annually [1, 2]. The disease can also significantly impact wildlife including, for example, several deer species, American bison (*Bison bison*), African buffalo (*Syncerus caffer*), the brushtail possum (*Trichosurus vulpecula*) and the European badger (*Meles meles*) [3-6]. The etiological agent of bTB is *Mycobacterium bovis*, a pathogen with a genome sequence that is 99.95% identical to *M. tuberculosis*, the primary cause of human tuberculosis (TB) [7]. In certain agroecological milieus *M. bovis* can also cause zoonotic TB with serious implications for human health [8-10].

Previous studies have shown that the pathogenesis of bTB disease in animals is similar to TB disease in humans and many of the features of *M. tuberculosis* infection are also characteristic of *M. bovis* infection in cattle [11-13]. Transmission is via inhalation of contaminated aerosol droplets and the primary site of infection is the lungs where the bacilli are phagocytosed by alveolar macrophages, which normally can contain or destroy intracellular bacilli [14, 15]. Disease-causing mycobacteria, however, can persist and replicate within alveolar macrophages via a bewildering range of evolved mechanisms that subvert and interfere with host immune responses [16-19]. These mechanisms include: recruitment of cell surface receptors on the host macrophage; blocking of macrophage phagosome-lysosome fusion; detoxification of reactive oxygen and nitrogen intermediates (ROI and RNI); harnessing of intracellular nutrient supply and metabolism; inhibition of apoptosis and autophagy; suppression of antigen presentation; modulation of macrophage signalling pathways; cytosolic escape from the phagosome; and induction of necrosis, which leads to immunopathology and shedding of the pathogen from the host [20-25].

Considering the dramatic perturbation of the macrophage by intracellular mycobacteria, we and others have demonstrated that bovine and human alveolar macrophage transcriptomes are extensively reprogrammed in response to infection with *M. bovis* and *M. tuberculosis* [26-31]. These studies have also revealed that differentially expressed gene sets and dysregulated cellular networks and pathways are functionally associated with many of the macrophage processes described above that can control or eliminate intracellular microbes.

For many intracellular pathogens it is now also evident that the infection process involves alteration of epigenetic marks and chromatin remodelling that may profoundly alter host cell gene expression [32-35]. For example, distinct DNA methylation changes are detectable in macrophages infected with the intracellular protozoan *Leishmania donovani*, which causes visceral leishmaniasis [36]. Recent studies using cells with a macrophage phenotype generated from the THP-1 human monocyte cell line have provided evidence that infection with *M. tuberculosis* induces alterations to DNA methylation patterns at specific inflammatory genes [37] and across the genome in a non-canonical fashion [38].

With regards to host cell histones, the intracellular pathogen *Chlamydia trachomatis* secretes NEU, a SET domain-containing effector protein that functions as a histone methyltransferase and induces chromatin modifications favourable to the pathogen [39]. It has also been shown that *Legionella pneumophila*—the causative agent of Legionnaires' disease—secretes a SET domain-containing histone methyltransferase, RomA, which targets histone H3 to downregulate host genes and promote intracellular replication [40]. In the context of mycobacterial infections, Yaseen et al. have shown that the Rv1988 protein, secreted by virulent mycobacteria, localises to the chromatin upon infection and mediates repression of host cell genes through methylation of histone H3 at a non-canonical arginine residue [41]. In addition, chromatin immunoprecipitation sequencing (ChIP-seq) analysis of H3K4 monomethylation (a marker of poised or active enhancers), showed that regulatory

96 sequence motifs embedded in subtypes of Alu SINE transposable elements are key
97 components of the epigenetic machinery modulating human macrophage gene expression
98 during *M. tuberculosis* infection [42].

99 In light of the profound macrophage reprogramming induced by mycobacterial
100 infection, and previous work demonstrating a role for host cell chromatin modifications, we
101 have used ChIP-seq and RNA sequencing (RNA-seq) to examine gene expression changes
102 that reflect host-pathogen interaction in bovine alveolar macrophages (bAM) infected with *M.*
103 *bovis*. The results obtained support an important role for dynamic chromatin remodelling in
104 the macrophage response to mycobacterial infection, particularly with respect to M1/M2
105 polarisation. Genes identified from ChIP-seq and RNA-seq results were also integrated with
106 GWAS data to prioritise genomic regions and SNPs associated with bTB resilience. Finally,
107 the suitability of bAM for ChIP-seq assays and the results obtained demonstrate that these
108 cells represent an excellent model system for unravelling the epigenetic and transcriptional
109 circuitry perturbed during mycobacterial infection of vertebrate macrophages.

110

111 # Results

112 ## *M. bovis* infection induces trimethylation of H3K4 at key immune function
113 related loci in bovine alveolar macrophages

114 Previous studies have shown that bAM undergo extensive gene expression
115 reprogramming following infection of *M. bovis* [29], with approximately one third of the
116 genome significantly differentially expressed within bovine macrophages 24 hours after
117 infection [28]. Changes of this magnitude are comparable to those observed in previous
118 experiments that have examined the chromatin remodelling that accompanies mycobacterial
119 infection of macrophages, where trimethylation of lysine 4 of Histone H3 (H3K4me3) was
120 shown to correlate with active transcription [42, 43].

121 We used chromatin immunoprecipitation sequencing (ChIP-seq) to examine histone
122 modification changes that occur after *M. bovis* infection of bAM from sex- and aged-matched
123 Holstein-Friesian cattle. The aim was to determine genome-wide changes in the distribution
124 of H3K4me3 and H3K27me3, and PolII occupancy at the response genes [44]. After data
125 quality control and filtering, ~760 million paired end reads were aligned to the UMD 3.1
126 bovine genome build at an average alignment rate of 96.23%. Correlation plots of genome-
127 wide H3K4me3, H3K27me3 and PolII sequencing reads from infected and non-infected
128 bAMs showed high correlation between samples (Pearson's correlation coefficient: 0.93–
129 0.97) for all three ChIP-seq targets (supplementary figure 1); indicating that the observed
130 differences in histone modifications between samples are limited and localised to specific
131 regions of the genome.

132 Differential peaks between conditions were called, compared and visualised with IGV
133 to determine where differences in H3K4me3, H3K27me3 and PolII occupancy occur between
134 control and infected bAM (Figure 1). ChIP seq peaks are defined as areas of the genome
135 enriched by read counts after alignment to the reference genome.

136 Peak differences for H3K4me3 occurred at multiple locations across the genome and
137 were estimated by the fold enrichment of a peak normalised against input control DNA that
138 had not undergone antibody enrichment. Differential peaks in each condition were defined by
139 several criteria: 1) the fold enrichment of each peak had to be larger than 10 in at least one
140 condition [45]; 2) the identified peaks had a *P*-value cut off of 0.05; 3) the peaks being
141 compared in each condition were no more than 500 bp up- and downstream of each other; 4)
142 the peaks were classified as different using log-likelihood ratios and affinity scores, with
143 using MACS2 and diffBind, respectively; and 5) visual inspection of the tracks of the peaks
144 confirmed the computationally determined differences in each condition.

145 Peaks that occurred in a particular sample indicate that H3K4me3 and PolII are highly
146 correlated with condition (Figure 2A); this demonstrates that the differences in H3
147 modifications are a result of infection rather than genomic differences between animals.
148 Analysis of genome-wide H3K4me3 revealed significant peak differences between control
149 and infected samples at multiple sites in the genome under these criteria, with some of these
150 differences occurring at the transcriptional start site of 233 genes. (Figure 2 A-D and
151 supplementary figure 4). Supplementary figure 1 demonstrates that the differences in
152 H3K4me3 and Pol II peaks are minor, with cells from both conditions sharing most peaks and
153 differing by only 1.8–2.95% in peaks across the genome. Principal component analysis
154 (PCA) of the H3K4me3 mark and PolII data indicated that these H3K4me3 and PolII peak
155 differences are strongly associated with *M. bovis* infection of bAM (supplementary figure 3).

156

157 **Changes in H3K4me3 are accompanied with immune related transcriptional**
158 **reprogramming**

159 Previous studies have shown that increased H3K4me3 is frequently accompanied by an
160 increase in PolII occupancy and elevated expression of proximal genes [46, 47]. In the
161 present study, we observed that H3K4me3 is accompanied by an increase in PolII occupancy
162 (Figure 1 and supplementary figure 4). For a small number of genes (24 out of 233) where the
163 H3K4me3 peak was larger in the control than the infected samples, PolII occupancy was
164 greater in control bAM for 20 genes (83.3%) and greater in infected bAM for three genes
165 (12.5%). Conversely, where the H3K4me3 peak was larger in the infected bAM, PolII
166 occupancy was greater in the infected samples for 127 genes (60.4%) and greater in the
167 control bAM for 14 genes (6.6%). The remaining 60 genes (25%) did not exhibit H3K4me-
168 associated PolII occupancy in either control or infected samples. Figure 3A illustrates this
169 trend, showing that PolII occupancy normally accompanies H3K4me3.

170 To establish if H3K4me3 mark patterns were correlated with changes in gene
171 expression, control non-infected bAM and bAM infected *M. bovis* AF2122/97 from four
172 animals 24 hpi (including the two animals used for ChIP-seq) were used to generate eight
173 RNA-seq libraries. After quality control and filtering, ~250 million reads were mapped to the
174 bovine genome, with 72% total read mapping, overall. RNA-seq analysis revealed 7,757
175 differentially expressed genes ($\log_2 FC > 0$: 3,723 genes; $\log_2 FC < 0$: 4,034 genes; FDR <
176 0.1). Of the 233 genes identified in the ChIP-seq analysis, 232 (99.6%) were differentially
177 expressed with these criteria (see supplementary file 2). Of the genes that exhibited
178 H3K4me3 peaks that were larger in the infected bAMs, 21 (10%) were downregulated and
179 189 (90%) were upregulated. Of the genes that exhibited larger H3K4me3 peaks in the
180 control group, 22 (91.6%) were downregulated and 2 (8.4%) were upregulated (Figure 3A).

181 This pattern of directional gene expression correlating with H3K4me3 for the control and
182 infected samples is consistent with the literature [46, 47].

183 Existing published RNA-seq data generated by our group using *M. bovis*-infected (*n* =
184 10) and control non-infected bAM (*n* = 10) at 24 hpi [29], was also examined in light of the
185 results from the present study. For the 232 genes identified here, a Pearson correlation
186 coefficient of 0.85 was observed for two data sets (Figure 3D), thus demonstrating that gene
187 expression differences between *M. bovis*-infected and control non-infected bAM are
188 consistent across experiments, even where samples sizes are markedly different.

189

190 Transcriptional reprogramming is coupled with differential microRNA 191 expression

192 We have previously demonstrated that differential expression of immunoregulatory
193 microRNAs (miRNAs) is evident in bAM infected with *M. bovis* compared to non-infected
194 control bAM [31, 48]. To investigate the expression of miRNA in bAM used for the ChIP-
195 seq analyses, miRNA was extracted and sequenced from the samples used for the RNA-seq
196 analysis. After quality control and filtering, ~100 million reads were mapped to the bovine
197 genome, with 79% total reads mapping, overall. Twenty-three differentially expressed
198 miRNAs were detected at 24 hpi ($\log_2$FC > 0: 13; $\log_2$FC < 0: 10; FDR < 0.10). Of the 232
199 genes identified in the ChIP-seq/RNA-seq analysis, 93 are potential targets for the 23
200 differentially expressed miRNAs (supplementary data 3). Further examination revealed that
201 multiple immune genes, such as *BCL2A1* (bta-mir-874), *ARG2* (bta-mir-101), *TMEM173*
202 (aka *STING*) (bta-mir-296-3p) and *STAT1* (bta-mir-2346), are potential regulatory targets for
203 these miRNAs (Figure 3B). This observation therefore supports the hypothesis that miRNAs
204 function in parallel with chromatin modifications to modulate gene expression in response to
205 infection by *M. bovis*.

206 The H3K4me3, PolII, K27me3 and RNA-seq data were subsequently integrated to
207 evaluate the relationship between histone modifications and gene expression changes. Three
208 dimensional plots were generated to visualize the global differences between H3K4me3,
209 PolII and gene expression in infected and non-infected bAM (Figure 3D). These plots show
210 that reduction of H3K4me3 in infected cells is associated with a decrease in gene expression
211 and an absence of PolII occupancy. Genome-wide H3K27me3 was also investigated to
212 determine whether methylation of this residue was altered in response to *M. bovis* infection
213 and if it was related to gene expression. No significant differences for H3K27me3 between
214 control and infected bAM were detected, indicating that repression of gene expression
215 through H3K27me3 does not play a role in the bAM response to *M. bovis* at 24hpi. However,
216 supplementary figure 2 indicates that the presence of a H3K27me3 peak in both control and
217 infected cells at the TSS of a H3k4me3 enriched gene correlated well with a lower or
218 complete lack of Pol II occupancy.

219

220 Pathway analysis reveals H3K4me3 marks are enriched for key 221 immunological genes

222 To identify biological pathways associated with genes identified through the ChIP-seq
223 analyses, we integrated the ChIP-seq, RNA-seq and miRNA-seq data and created a list of 232
224 genes that were present in each data set. Pathway analyses were carried out using three
225 pathway tools: Ingenuity Pathway Analysis (IPA), Panther and DAVID [49-51]. IPA
226 revealed an association with *respiratory illness* and the *innate immune response*
227 (supplementary file 2). Panther was used to examine the gene ontology categories of the 232
228 genes (Figure 4A); this revealed enrichment for metabolic processes, response to stimuli and
229 cellular processes, indicating that increased H3K4me3 in response to *M. bovis* infection
230 occurs at TSS of genes associated with the immune response.

231 The final part of the pathway analysis was performed using DAVID [51]. DAVID uses
232 a list of background genes and query genes (in this case the 232 common genes across data
233 sets) and identifies enriched groups of genes with shared biological functions. The DAVID
234 analysis demonstrated that the 232 genes are involved in several signalling pathways,
235 including the PI3K/AKT/mTOR, JAK-STAT and RIG-I-like signalling pathways (Figure 4B
236 and the top 10 pathways are detailed in supplementary file 3).

237

238 GWAS integration prioritises bovine SNPs associated with resilience to *M.* 239 *bovis* infection

240 Previous work used high-density SNP (597,144 SNPs) data from 841 Holstein-
241 Friesian bulls for a genome-wide association study (GWAS) to detect SNPs associated with
242 susceptibility/resistance to *M. bovis* infection [52]. Using a permutation-based approach to
243 generate null SNP distributions, we leveraged these data to show that genomic regions within
244 100 kb up- and downstream of each of the 232 genes exhibiting differential H3K4me3 ChIP-
245 seq peaks are significantly enriched for additional SNPs associated with resilience to *M. bovis*
246 infection.

247 In total, 12,056 SNPs within the GWAS data set were located within 100 kb of the
248 232 H3K4me3 genes. Of these SNPs, up to 26 were found to be significantly associated with
249 bTB susceptibility, depending on the distance interval of each gene. Interestingly, 22 SNPs
250 found within 25 kb of 11 genes were found to be most significant at P and q values < 0.05,
251 with declining significance of association as the region extended beyond 25 kb (Figure 4C
252 and supplementary file 3). Significant SNPs were detected in proximity to the following
253 genes: *SAMSN1, CTSL, TNFAIP3, CLMP, ABTB2, RNFT1, MIC1, MIC2, EDN1, ARID5B*,
254 all of which had significant differential enrichment of H3K4me3.

255 # Discussion

256 ## H3K4me3 mark occurs at key immune genes

257 Our study has generated new information regarding host-pathogen interaction during
258 the initial stages of *M. bovis* infection. We demonstrate that chromatin is remodelled through
259 differential H3K4me3 and that PolII occupancy is altered at key immune genes in *M. bovis*-
260 infected bAM. This chromatin remodelling correlates with changes in the expression of genes
261 that are pivotal for the innate immune response to mycobacteria [28, 29, 53]. Our work
262 supports the hypothesis that chromatin modifications of the host macrophage genome play an
263 essential role during intracellular infections by mycobacterial pathogens [54, 55].

264 The top pathways identified were the JAK-STAT signalling pathway, the
265 PI3K/AKT/mTOR signalling pathway and the RIG-I-like receptor signalling pathway. In
266 mammals, the JAK-STAT pathway is the principal signalling pathway that modulates
267 expression of a wide array of cytokines and growth factors, involved in cell proliferation and
268 apoptosis [56]. The JAK-STAT signalling pathway and its regulators are also associated with
269 coordinating an effective host response to mycobacterial infection [57, 58]. Two JAK-STAT
270 associated stimulating factors and a ligand receptor that exhibited increased H3K4me3 marks
271 in infected samples were encoded by the *OSM*, *CSF3* and *CNTFR* genes, respectively [59,
272 60]. *OSM* has previously been shown to be upregulated in cells infected with either *M. bovis*
273 or *M. tuberculosis* [29, 61, 62]. Our work shows that this increased expression in response to
274 mycobacteria is facilitated by H3K4me3-mediated chromatin accessibility. The protein
275 encoded by *CSF3* has also been implicated as an immunostimulator in the response to
276 mycobacterial infection due to its role in granulocyte and myeloid haematopoiesis [63].
277 *CNTFR* encodes a ligand receptor that stimulates the JAK-STAT pathway and shows
278 increased expression in other studies of mycobacterial infection [28, 29]. Following
279 stimulation of *JAK* through ligand receptor binding, *STAT1* expression is increased. STAT1,

280 a signal transducer and transcription activator that mediates cellular responses to interferons
281 (IFNs), cytokines and growth factors, is a pivotal JAK-STAT component and a core
282 component in the response to mycobacterial infection [64]. Here, the TSS of *STAT1* was
283 associated with an increased deposition of H3K4me3. Interestingly, upregulation of *STAT1*
284 was associated with a downregulation of bta-miR-2346, predicted to be a negative regulator
285 of STAT1 (see supplementary file 3). Overall, these results show that major components of
286 the JAK-STAT pathway undergo chromatin remodelling mediated via H3K4me3, thereby
287 facilitating activation and propagation of the JAK-STAT pathway through chromatin
288 accessibility.

289 Key genes encoding components of the PI3K/AKT/mTOR pathway, such as *IRF7*,
290 *RAC1* and *PIK3AP1*, were also identified as having increased H3K4me3 in *M. bovis* infected
291 macrophages. PI3K/AKT/mTOR signalling contributes to a variety of processes that are
292 critical in mediating aspects cell growth and survival [65]. Phosphatidylinositol-3 kinases
293 (PI3Ks) and the mammalian target of rapamycin (mTOR) are integral to coordinating innate
294 immune defences [66]. The PI3K/AKT/mTOR pathway is an important regulator of type I
295 interferon production via activation of the interferon-regulatory factor 7, IRF7. RAC1 is a
296 key activator of the PI3K/AKT/mTOR pathway and, in its active state, binds to a range of
297 effector proteins to regulate cellular responses such as secretory processes, phagocytosis of
298 apoptotic cells, and epithelial cell polarization [67]. In addition, *in silico* analysis of our
299 differentially expressed miRNAs predicted that several miRNAs, such as bta-miR-1343-3p,
300 bta-miR-2411-3p and bta-miR-1296, regulate *RAC1*. *PIK3AP1* expression was also
301 increased, in line with previous mycobacterial infection studies [28, 29]. Hence as observed
302 with the JAK-STAT pathway, H3K4me3 at these key PI3K/AKT/mTOR pathway genes acts
303 to regulate the innate response to mycobacterial infection.

304 Initiation of the RIG-I-like receptor signalling pathway generally occurs following viral
305 infection through sensing of viral RNAs by cytoplasmic RIG-I-like receptors (RLRs) and
306 activation of transcription factors that drive production of type I IFNs [68]. A number of
307 bacterial species induce type I IFN independently of TLRs, potentially through the RIG-I-like
308 pathway [69, 70]. While type I IFNs have a well characterised role in the inhibition of viral
309 replication, their role during bacterial infection is less well defined [71-73]. In humans and
310 mice, *M. tuberculosis*-induced type I IFN is associated with TB disease progression and
311 impairment of host resistance [74-76]. In our study, genes encoding multiple components of
312 the RIG-I-like receptor signalling pathway, such as *TRIM25, ISG15, IRF7* and *IKBKE,* were
313 enriched for K4me3 and PolII occupancy in *M. bovis*-infected bAM. These results
314 demonstrate that the RIG-I-like pathway activation in *M. bovis*-infected bAM is driven, to a
315 large extent, by reconfiguration of the host chromatin.

316 H3K4me3 enriched loci are also flanked by genomic polymorphisms associated with
317 resilience to *M. bovis* infection. Integration of our data with GWAS data from 841 bulls that
318 have robust phenotypes for bTB susceptibility/resistance revealed 22 statistically significant
319 SNPs within 25 kb of 11 H3K4me3 enriched genes. Most of these genes are involved in host
320 immunity, with *CTSL, TNFAIP3,* and *RNFT1* directly implicated in the human response to
321 *M. tuberculosis* infection [77-79]. The reprioritisation of genomic regions and array-based
322 SNPs using integrative genomics approaches will be relevant for genomic prediction and
323 genome-enabled breeding and may facilitate fine mapping efforts and the identification of
324 targets for genome editing of cattle resilient to bTB.

325

326 **H3K4me3 deposition at host macrophage genes and immunological evasion**
327 **by *M. bovis***

328 The present study has revealed elevated H3K4me3 deposition and PolII occupancy at
329 key immune genes that are involved in the innate response to mycobacterial infection. In
330 addition, we also identified several immune genes that had differential H3K4me3 and
331 expression, where the expression change may be detrimental to the ability the host
332 macrophage to clear infection. An example of this is *ARG2*, which exhibited increased
333 H3K4me3 deposition, PolII occupancy and expression ($Log_2FC = 3.415$, $P_{adj} = 7.52 \times 10^{-16}$)
334 in infected cells. However, it is also interesting to note that the integrated expression output
335 of *ARG2* may also be determined by the bta-miR-101 miRNA, a potential silencer of *ARG2*
336 expression, which was observed to be upregulated in infected cells. Elevated levels of
337 arginase 2, the protein product of the *ARG2* gene, have previously been shown to shift
338 macrophages to an M2 phenotype [80, 81], which is anti-inflammatory and exhibits
339 decreased responsiveness to IFN-gamma and decreased bactericidal activity [82]. Hence, it
340 may be hypothesised that *M. bovis* infection triggers H3K4me3 deposition at the TSS of
341 *ARG2* to drive an M2 phenotype and generate a more favourable niche for the establishment
342 of infection. Similarly to *ARG2,* increased expression of *BCL2A1* in *M. bovis*-infected bAM
343 may also facilitate development of a replicative milieu for intracellular mycobacteria.
344 Increased expression of *BCL2A1* is associated with decreased macrophage apoptosis [83],
345 which would otherwise restrict replication of intracellular pathogens.

346 In comparison to control non-infected bAM, the *TMEM173* (aka *STING*) gene
347 exhibited substantially decreased expression in *M. bovis*-infected bAM ($Log_2FC = -3.225$,
348 $P_{adj} = 8.64 \times 10^{-11}$). *TMEM173* encodes transmembrane protein 173, which drives IFN
349 production and as such is a major regulator of the innate immune response to viral and
350 bacterial infections, including *M. bovis* and *M. tuberculosis* [28, 84, 85]. Downregulation of

351 *TMEM173* indicates that *M. bovis* can actively reduce or block methylation of H3K4 at this
352 gene in infected macrophages, thereby enhancing the pathogen's intracellular survival. In this
353 regard, we have recently shown that infection of bAM with *M. tuberculosis*, which is
354 attenuated in cattle, causes increased *TMEM173* expression compared to infection with *M.*
355 *bovis* [28].

356 The molecular mechanisms that pathogens employ to manipulate the host genome to
357 subvert or evade the immune response are yet to be fully elucidated. Hijacking the host's own
358 mechanisms for chromatin modulation is one potential explanation that has garnered attention
359 in recent years [33, 35]. These modulations of the host chromatin in bAMs may be mediated
360 through *M. bovis*-derived signals transmitted through bacterial metabolites, RNA-signalling
361 or secreted peptides [41, 86-88].

362 Conclusions

363 Elucidation of the mechanisms used by pathogens to establish infection, and ultimately
364 cause disease, requires an intimate knowledge of host-pathogen interactions. Using
365 transcriptomics and epigenomics, we have identified altered expression of major host
366 immune genes following infection of primary bovine macrophages with *M. bovis.* We have
367 shown that reprogramming of the alveolar macrophage transcriptome occurs mainly through
368 increased deposition of H3K4me3 at key immune function genes, with additional gene
369 expression modulation via miRNA differential expression. This modulation of gene
370 expression drives a shift of the macrophage phenotype towards the more replicate-permissive
371 M2 macrophage phenotype. We have also identified that alveolar macrophages infected with
372 *M. bovis* exhibit differentially expressed genes (in regions with modified chromatin) that are
373 enriched for significant SNPs from GWAS data for bTB resilience; this shows the power of
374 integrative approaches to identify key loci to be targeted for selective breeding programmes.

375 Our data confirm the emerging concept that pathogens can hijack host chromatin, through
376 manipulation of H3K4me3, to subvert host immunity and to establish infection.

377 # Methods

378 ## Preparation and infection of bAMs

379 Alveolar macrophages and *M. bovis* 2122 were prepared as described previously [89]
380 with minor adjustments, 2×10^6 macrophages were seeded in 60 mm tissue culture plates and
381 challenged with *M. bovis* at an MOI of 10:1 (2×10^7 bacteria per plate) for 24 h; parallel non-
382 infected controls were prepared simultaneously.

383

384 ## Preparation of nucleic acids for sequencing

385 Sheared fixed chromatin was prepared exactly as described in the truChIP™ Chromatin
386 Shearing Kit (Covaris) using 2×10^6 macrophage cells per AFA tube. Briefly, cells were
387 washed in cold PBS and 2.0 ml of fixing Buffer A was added to each plate, to which 200 µl
388 of freshly prepared 11.1% formaldehyde solution was added. After 10 min on a gentle rocker
389 the crosslinking was halted by the addition of 120 µl of quenching solution E, cells were
390 washed with cold PBS, released from the plate using a cell scraper and re-suspended in 300
391 µl Lysis Buffer B for 10 min with gentle agitation at 4ºC to release the nuclei. The nuclei
392 were pelleted and washed once in Wash Buffer C and three times in Shearing Buffer D3 (X3)
393 prior to been resuspended in a final volume of 130 µl of Shearing Buffer D3. The nuclei were
394 transferred to a micro AFA tube and sonicated for 8 min each using the Covaris E220e as per
395 the manufacturer's instructions. Chromatin immunoprecipitation of sonicated DNA samples
396 was carried out using the Chromatin Immunoprecipitation (ChIP) Assay Kit (Merck KGaD)
397 and anti-H3K4me3 (05-745R) (Merck KGaD), Pol II (H-224) (Santa Cruz Biotechnology,
398 Inc.) or anti-H3K27me3 (07-449) (Merck KGaD) as previously described [90]. RNA was
399 extracted from infected (n = 4) and control (n = 4) bAM samples using the RNeasy Plus Mini

400 Kit (Qiagen) as previously described [91]. All 8 samples exhibited excellent RNA quality
401 metrics (RIN >9).

402

403 ## Sequencing

404 Illumina TruSeq Stranded mRNA and TruSeq Small RNA kits were used for mRNA-
405 seq and small RNA-seq library preparations and the NEB Next Ultra ChIPseq Library Prep
406 kit (New England Biolabs) was used for ChIP-seq library preparations. Pooled libraries were
407 sequenced by Edinburgh Genomics (http://genomics.ed.ac.uk) as follows: paired-end reads (2
408 × 75 bp) were obtained for mRNA and ChIP DNA libraries using the HiSeq 4000 sequencing
409 platform and single-end read (50 bp) were obtained for small RNA libraries using the HiSeq
410 2500 high output version 4 platform.

411

412 ## ChIP-seq bioinformatics analysis

413 Computational analyses for all bioinformatic processes were performed on a 72-CPU
414 compute server with Linux Ubuntu (version 16.04.4 LTS). An average of 54 M paired end
415 75bp reads were obtained for each histone mark. At each step of data processing, read quality
416 was assessed via FastQC (version 0.11.5) [92]. Any samples that indicated adapter
417 contamination were trimmed via Cutadapt (version 1.15) [93]. Raw read correlation plots
418 were generated via EaSeq (version 1.05) [94]. The raw reads were aligned to UMD 3.1.1
419 bovine genome assembly using Bowtie2 (version 2.3.0) [95]. The mean alignment rate for the
420 histone marks was 96.23%. The resulting SAM files were converted and indexed into BAM
421 files via Samtools (version 1.3.1) [96]. After alignment, samples were combined and sorted
422 into 14 files, based on the animal (A1 or A2), the histone mark (K4/K27/PolII) and treatment
423 (control or infected) i.e. A1-CTRL-K4. Peaks were called by using alignment files to

424 determine where the reads have aligned to specific regions of the genome, and then
425 comparing that alignment to the input samples as a normalization step.

426 The peak calling was carried out via MACS (version 2.1.1.20160309) [97]. The K4me3
427 mark was called in sharp peak mode and K27me3 and Pol II were called in broad peak mode,
428 as per the user guide. Peak tracks were generated in macs and visualized with the Integrative
429 Genome Viewer (version 2.3) [98]. Union peaks were generated by combining and merging
430 overlapping peaks in all samples for each histone mark. Differential peak calling was called
431 via macs using the bdgdiff function. Peaks images were generated by visually assessing all
432 three marks in tandem across the entire bovine genome with IGV. The significance of peaks
433 was determined by sorting peaks for each mark in each treatment by *P* value and then fold
434 enrichment with a cut-off of 2 and a *P* value threshold of 0.05 [99]. Peaks from each animal
435 in each condition for each mark were cross referenced with the IGV images and differential
436 peak caller to determine a difference in fold enrichment for each observed peak difference
437 between conditions. This required comparing peak start and end sites, chromosomes, *P* and *q*
438 values for each summit, summit locations and normalised fold enrichment of a peak against
439 the input sample (see supplementary file 1 for peak sets). Any peaks that exhibited a
440 difference of 4 or greater fold enrichment, a *P* value of less than 0.05, an FDR (*q* value) less
441 than 0.05 and that were also identified by the differential peak caller were selected for further
442 analysis (see supplementary file 1 for peaks at TSS that met some but not all of the above
443 criteria). Peaks that were then classified to be different between conditions in all three data
444 sets were examined to determine their proximity to TSS. Differential peaks were also called
445 using the R package DiffBind (version 2.80) [100]. DiffBind includes functions to support
446 the processing of peak sets, including overlapping and merging peak sets, counting
447 sequencing reads overlapping intervals in peak sets, and identifying statistically significantly
448 differentially bound sites based on evidence of binding affinity (measured by differences in

449 read densities, see supplementary info 1). For H3K27me3 DiffBind differential peak calling,
450 the initial MACS2 peak list, consisting of 64,264 total peaks (see supplementary info 1), was
451 merged and reduced to a smaller group of larger, broader peaks to reduce noise and false
452 positive discovery (Figure 2B).

453

454 **RNA-seq bioinformatics analysis**

455 An average of 44 M paired end 75 bp reads were obtained for each of the eight samples
456 (four control, four infected). Adapter sequence contamination and paired-end reads of poor
457 quality were removed from the raw data. At each step, read quality was assessed with FastQC
458 (version 0.11.5). Any samples that indicated adapter contamination were trimmed via
459 Cutadapt (version 1.15). The raw reads were aligned to the UMD 3.1.1 bovine transcriptome
460 using Salmon (version 0.8.1) [101]. Aligned reads were also counted in Salmon and the
461 resulting quantification files were annotated at gene level via tximport (version 3.7) [102].
462 The annotated gene counts were then normalised and differential expression analysis
463 performed with DESeq2 (version 1.20.0) [103], correcting for multiple testing using the
464 Benjamini-Hochberg method [104]. Genes identified from ChIP-seq as exhibiting differential
465 histone modifications were cross referenced with the RNA-seq data set to determine
466 significant $\log_2$FC between *M. bovis*-infected and control non-infected. Additionally, this
467 RNA-seq data was cross referenced with RNA-seq data from a previous study that
468 investigated bAM infected with *M. bovis* [29].

469

470 **MicroRNA-seq bioinformatics analysis**

471 A mean of 26 M paired-end 50 bp reads were obtained for each of the eight samples
472 (four control, four infected). At each step of data processing, read quality was assessed via

473 fastqc (version 0.11.5). Any samples that exhibited adapter contamination were trimmed via
474 Cutadapt (version 1.15) and all reads smaller than 17 bp were removed from the analysis.
475 Raw reads were mapped to UMD3.1 using Bowtie (version 1.2.2). miRNA detection,
476 identification and quantification was carried out with mirdeep2 (version 0.0.91). Isoform
477 analysis was also performed using mirdeep2. Differential expression analysis was performed
478 using DESeq2, correcting for multiple testing with the Benjamini-Hochberg method. Any
479 miRNAs that were significantly differentially expressed (FDR < 0.10) were selected for
480 further analysis. To determine if significantly differentially expressed miRNAs target genes
481 selected in the ChIP seq analysis, miRmap [105] was used to predict the likelihood a specific
482 miRNA targets one or more of the genes based on three criteria: delta G binding, probability
483 exact and phylogenetic conservation of seed site, which is then combined into a single
484 scoring metric (miRmap score). Any predicted gene targets with miRmap score ≥ 0.70 were
485 included in the analysis (see supplementary info 3).

486

487 **Pathway analysis**

488 Pathway analysis was carried out on any gene that had a differential peak between
489 control and infected samples. Pathway analysis and gene ontology was carried out by DAVID
490 (version 6.8), Ingenuity pathway analysis (01-13) and PANTHER (version 13.1) [49, 106].
491 KEGG pathways were selected by choosing pathways that had the highest number of genes
492 identified in the ChIP seq data and had a FDR < 0.05.

493

494 **Integration of GWAS data.**

495 GWAS data for genetic susceptibility to *M. bovis* infection previously generated by
496 Richardson and colleagues [52] were analysed to determine if subsets of SNPs selected

497 according to their distance to H3K4me3 and PolII active loci were enriched for significant
498 GWAS hits. The nominal *P* values used in this study were generated using single SNP
499 regression analysis in a mixed animal model as described previously [52]. In summary, high-
500 density genotypes (n = 597,144) of dairy bulls (n = 841) used for artificial insemination were
501 associated with deregressed estimated breeding values for bTB susceptibility that had been
502 calculated from epidemiological information on 105,914 daughters and provided by the Irish
503 Cattle Breeding Federation (ICBF). In this study, the significance of the distribution of SNP
504 nominal *P* values (from Richardson et al 2016) within and up to 100 kb up and downstream
505 to genes identified as having differential H3K4me3 and PolII activity on bTB susceptibility
506 were estimated in R using *q* value (FDRTOOL) and permutation analysis (custom scripts). A
507 total of 1000 samplings (with replacement) from the HD GWAS *P* value data set (n =
508 597,144) representing the size of each of selected SNP subsets were generated. The *q* values
509 for each SNP *P* value subset and all its permuted equivalents were calculated using the
510 FDRTOOL library in R. The subsequent significance level (P_{perm}) assigned to each of the
511 SNP subsets was equivalent to the proportion of permutations in which at least the same
512 number of *q* values < 0.05 as the SNP subset were obtained, i.e. by chance.

513 # Figure legends

514 **Figure 1. Track visualization of *M. bovis* induced H3K4me3 and PolII occupancy with**
515 **relative change in expression at three immune response associated genes.**

516 Examples of signal tracks illustrating peaks of H3K27me3 (top two tracks), H3K4me3
517 (middle two tracks) and PolII (bottom two tracks) in infected (red) and non-infected (blue)
518 bovine alveolar macrophages, with the bovine reference genome on the bottom of each panel
519 reading left to right. Accompanying each track image is the expression of the corresponding
520 gene, with normalised counts of infected cells in red and control in blue. The *ARG2* gene
521 exhibited an increase in H3K4me3 at 24 hpi as evidenced by the larger red H3K4me3 and red
522 PolII peaks. The *IFITM2* gene also exhibited larger H3K4me3 and PolII peaks in infected
523 samples; however, in contrast to this, *SIRT3*, which is located ~20kb upstream from *IFITM2*
524 gene, had no significant change in either peak. *TMEM173* (aka *STING*) exhibits an opposite
525 pattern to most genes identified as having differential H3K4me3, where a larger peak is
526 observed in control samples rather than infected.

527

528 **Figure 2. *M.bovis* induced histone modifications occur genome wide at key immune loci.**

529 (**A**) Correlation heatmaps of differential peaks for H3K4me3, H3K27me3 and PolII. Every
530 peak location that is not consistent between each animal in each condition (i.e. a peak only
531 occurs in the control group) is compared to determine if these inconsistent peaks are
532 correlated with the animal or the condition. The differential peaks in H3K4me3 and PolII
533 correlate highly with condition, whereas there was no significant global differences in the
534 distribution of H3K27me3. (**B**) Venn diagrams of differential peaks for H3K4me3,
535 H3K27me3 and PolII. Each condition shares the majority of peaks. Where differences occur
536 at TSS of genes, these genes are frequently associated with immune function. (**C**) Volcano

537 plots of differential peaks for H3K4me3 and PolII. The y-axis shows significance as FDR and
538 the x-axis indicates increase in affinity for control (left) and infected (right). Significant sites
539 are denoted in blue. (**E**) Boxplots of differential peaks for H3K4me3 and PolII. Infected bAM
540 are shown in red and control bAM are shown in blue. The left two boxes of each plot show
541 distribution of reads over all differentially bound sites in the infected and control groups. The
542 middle two boxes of each plot show the distribution of reads in differentially bound sites that
543 increase in affinity in the control group. The far right boxes in each plot show the distribution
544 of reads in differentially bound sites that increase in affinity in the infected group.

545

546 **Figure 3. H3K4me3 is accompanied by functional changes in PolII occupancy, gene**
547 **expression and gene regulation.**

548 (**A**) Scatter plots of H3K4me3 against PolII occupancy and gene expression. The first plot is
549 the difference of peaks for H3K4me3 between conditions, ranging from negative to positive
550 values, with negative being a larger peak in the control samples (blue dots) and the positive
551 values being a larger peak in the infected samples (red dots), on the y-axis. The x-axis
552 represents the $\log_2$FC for each of the 232 genes, with each gene as a single data point. The
553 second plot also has H3K4me3 on the y-axis but with peak differences in PolII on the x-axis,
554 with negative and positive values corresponding to greater occupancy in the control and
555 infected samples, respectively. The final plot shows $\log_2$FC relative to PolII occupancy. (**B**)
556 Plots of normalised miRNA-seq counts. Each plot represents the normalised counts of a
557 miRNA that was detected as exhibiting differential expression. Bta-miR-101 interacts with
558 *ARG2*, bta-miR-296-3p with *TMEM173* (aka *STING*), bta-miR-874 with *BCL2A1* and bta-
559 miR-2346 with *STAT1*. Red bars indicate infected and blue represent control samples.
560 (**C**) Correlation and Venn diagram for both RNA-seq studies. The x-axis of the scatter plot

561 represents the log_2FC for each of the 232 genes from this study and the y-axis represents the
562 log_2FC for each of the 232 genes from the previous study [29]. The Venn diagram shows the
563 global overlap of differentially expressed genes from both studies with an FDR cut off of
564 <0.1. (**D**) 3-D plots for all three data sets. A combination of all three scatter plots from Figure
565 2A. Data points are genes. Blue genes are those that exhibited greater H3K4me3 in control
566 bAM, red exhibited greater H3K4me3 in infected bAM.

567

568 **Figure 4. Gene ontology enrichment and pathway analysis.**

569 (**A**) Gene ontology pie charts generated through PANTHER pathway analysis. 232 genes
570 cluster by gene ontology under three main categories: *Biological process*, *Cellular*
571 *component* and *Molecular function*. (**B**) KEGG pathway images containing genes identified
572 from the ChIP-seq and RNA-seq analysis. Gene symbols coloured in yellow were identified
573 in the ChIP-seq and RNA-seq analysis. Gene symbols coloured in red were also targeted by
574 one or more differentially expressed miRNAs. Up or down red arrows indicate greater
575 H3K4me3 in infected or control, respectively. Up or down yellow arrows indicate log2FC
576 increase or decrease of the associated gene, respectively. (**C**) Line graph showing different
577 genomic ranges from genes that are enriched for significant SNPs from GWAS data for bTB
578 resilience. The bars represent the number of SNPs that occupy each range from each ChIP-
579 seq enriched gene, with more SNPs correlating with a greater distance. The blue plotted line
580 represents the negative log_{10} probability that the significant SNPs found at each distance at
581 0.05 FDR q value are significant by chance, with SNPs at 25 kb exhibiting the lowest
582 probability. The null SNP P value distribution for each data point was generated from 1000
583 permutations of random SNPs corresponding to the number of SNPs observed in a particular
584 genomic range. (D) Genes enriched for SNPs significantly associated with resilience to *M.*

585 *bovis* infection. SNP IDs and functional information obtained from the GeneCards® database

586 [107] are also shown.

587

588 ## Abbreviations

589 bAM: bovine alveolar macrophage/s; bTB: bovine tuberculosis; ChIP: chromatin
590 immunoprecipitation; FDR: false discovery rate; GWAS: genome-wide association study;
591 H3K27me3: histone H3 lysine 27 tri-methylation; H3K4me3: histone H3 lysine 4 tri-
592 methylation; hpi: hours post infection; log_2FC: log_2 fold change; PolII: RNA Polymerase II;
593 SNP: single nucleotide polymorphism; TB: tuberculosis.

594 ## Acknowledgments

595 The authors would also like to thank FAANG–Europe for awarding A.M.O.D. a short-
596 term scientific mission (STSM) grant. We would also like to acknowledge Edinburgh
597 Genomics for generation of sequencing data.

598 ## Author Contributions

599 Conceptualization, A.M.O.D., D.E.M. and T.J.H.; Software and Formal Analysis,
600 T.J.H. and M.P.M.; Investigation, A.M.O.D., D.V. and J.A.B.; Resources, D.E.M., S.V.G.
601 and D.V.; Data Curation, T.J.H.; Writing – original draft, T.J.H, A.M.O.D. and D.E.M.;
602 Writing – review and editing, D.V., S.V.G and M.P.M.; Supervision and Project
603 Administration, D.E.M. and A.M.O.D.; Funding Acquisition; D.E.M, S.V.G, D.V. and
604 A.M.O.D.

605 ## Competing Interests

606 The authors declare no competing interests.

607 ## Ethics Statement and Consent to Participate

608 All animal procedures were performed according to the provisions of Statutory
609 Instrument No. 543/2012 (under Directive 2010/63/EU on the Protection of Animals used for
610 Scientific Purposes). Ethical approval was obtained from the University College Dublin

611 Animal Ethics Committee (protocol number AREC-13-14-Gordon). No human subjects were
612 used for this study.

613 **Consent for Publication**

614 Not applicable.

615

Funding

This study was supported by Science Foundation Ireland (SFI) Investigator Programme Awards to D.E.M. and S.V.G. (grant nos. SFI/08/IN.1/B2038 and SFI/15/IA/3154); a European Union Framework 7 Project Grant to D.E.M. (no: KBBE-211602-MACROSYS); an EU H2020 COST Action short-term scientific mission (STSM) grant to A.M.O.D. (reference code: COST-STSM-ECOST-STSM-CA15112-050317-081648); a University of Edinburgh Chancellor's Fellowship to D.V.; and Institute Strategic Grant funding to the Roslin Institute (grant nos. BBS/E/D/10002070 and BBS/E/D/20002172). The funding agencies had no role in the study design, collection, analysis, and interpretation of data, and no role in writing the manuscript.

627 ## References

628 1. Steele JH: **Introduction (Part 2 Regional and Country Status Reports).** In
629 *Mycobacterium bovis infection in animals and humans.* Edited by Thoen CO, Steele JH.
630 Ames, IA, USA: Iowa State University Press; 1995: 169-172

631 2. Waters WR, Palmer MV, Buddle BM, Vordermeier HM: **Bovine tuberculosis**
632 **vaccine research: historical perspectives and recent advances.** *Vaccine* 2012, **30:**2611-
633 2622.

634 3. Fitzgerald SD, Kaneene JB: **Wildlife reservoirs of bovine tuberculosis worldwide:**
635 **hosts, pathology, surveillance, and control.** *Vet Pathol* 2013, **50:**488-499.

636 4. Gormley E, Corner LAL: **Pathogenesis of *Mycobacterium bovis* infection: the**
637 **badger model as a paradigm for understanding tuberculosis in animals.** *Front Vet Sci*
638 2017, **4:**247.

639 5. Malone KM, Gordon SV: ***Mycobacterium tuberculosis* complex members adapted**
640 **to wild and domestic animals.** *Adv Exp Med Biol* 2017, **1019:**135-154.

641 6. Palmer MV: ***Mycobacterium bovis*: characteristics of wildlife reservoir hosts.**
642 *Transbound Emerg Dis* 2013, **60 Suppl 1:**1-13.

643 7. Garnier T, Eiglmeier K, Camus JC, Medina N, Mansoor H, Pryor M, Duthoy S,
644 Grondin S, Lacroix C, Monsempe C, et al: **The complete genome sequence of**
645 ***Mycobacterium bovis*.** *Proc Natl Acad Sci U S A* 2003, **100:**7877-7882.

646 8. Olea-Popelka F, Muwonge A, Perera A, Dean AS, Mumford E, Erlacher-Vindel E,
647 Forcella S, Silk BJ, Ditiu L, El Idrissi A, et al: **Zoonotic tuberculosis in human beings**
648 **caused by *Mycobacterium bovis* – a call for action.** *Lancet Infect Dis* 2017, **17:**e21-e25.

649 9. Thoen CO, Kaplan B, Thoen TC, Gilsdorf MJ, Shere JA: **Zoonotic tuberculosis. A**
650 **comprehensive ONE HEALTH approach.** *Medicina (B Aires)* 2016, **76:**159-165.

651 10. Vayr F, Martin-Blondel G, Savall F, Soulat JM, Deffontaines G, Herin F:
652 **Occupational exposure to human *Mycobacterium bovis* infection: A systematic review.**
653 *PLoS Negl Trop Dis* 2018, **12:**e0006208.

654 11. Buddle BM, Vordermeier HM, Hewinson RG: **Experimental infection models of**
655 **tuberculosis in domestic livestock.** *Microbiol Spectr* 2016, **4**.

656 12. Waters WR, Maggioli MF, McGill JL, Lyashchenko KP, Palmer MV: **Relevance of**
657 **bovine tuberculosis research to the understanding of human disease: historical**
658 **perspectives, approaches, and immunologic mechanisms.** *Vet Immunol Immunopathol*
659 2014, **159:**113-132.

660 13. Williams A, Orme IM: **Animal models of tuberculosis: an overview.** *Microbiol*
661 *Spectr* 2016, **4**.

662 14. Kaufmann SHE, Dorhoi A: **Molecular determinants in phagocyte-bacteria**
663 **interactions.** *Immunity* 2016, **44:**476-491.

664 15. Weiss G, Schaible UE: **Macrophage defense mechanisms against intracellular**
665 **bacteria.** *Immunol Rev* 2015, **264:**182-203.

666 16. Awuh JA, Flo TH: **Molecular basis of mycobacterial survival in macrophages.**
667 *Cell Mol Life Sci* 2017, **74:**1625-1648.

668 17. Schorey JS, Schlesinger LS: **Innate immune responses to tuberculosis.** *Microbiol*
669 *Spectr* 2016, **4**.

670 18. Cambier CJ, Falkow S, Ramakrishnan L: **Host evasion and exploitation schemes of**
671 ***Mycobacterium tuberculosis*.** *Cell* 2014, **159:**1497-1509.

672 19. de Chastellier C: **The many niches and strategies used by pathogenic**
673 **mycobacteria for survival within host macrophages.** *Immunobiology* 2009, **214:**526-542.

674 20. Stutz MD, Clark MP, Doerflinger M, Pellegrini M: ***Mycobacterium tuberculosis*:**
675 **Rewiring host cell signaling to promote infection.** *J Leukoc Biol* 2018, **103:**259-268.

676 21. Chaurasiya SK: **Tuberculosis: Smart manipulation of a lethal host.** *Microbiol*
677 *Immunol* 2018, **62:**361-379.

678 22. BoseDasgupta S, Pieters J: **Macrophage-microbe interaction: lessons learned from**
679 **the pathogen *Mycobacterium tuberculosis*.** *Semin Immunopathol* 2018, **40:**577-591.

680 23. Queval CJ, Brosch R, Simeone R: **The macrophage: A disputed fortress in the**
681 **battle against *Mycobacterium tuberculosis*.** *Front Microbiol* 2017, **8:**2284.

682 24. Hussain Bhat K, Mukhopadhyay S: **Macrophage takeover and the host-bacilli**
683 **interplay during tuberculosis.** *Future Microbiol* 2015, **10:**853-872.

684 25. Ehrt S, Schnappinger D: **Mycobacterial survival strategies in the phagosome:**
685 **defence against host stresses.** *Cell Microbiol* 2009, **11:**1170-1178.

686 26. Papp AC, Azad AK, Pietrzak M, Williams A, Handelman SK, Igo RP, Jr., Stein CM,
687 Hartmann K, Schlesinger LS, Sadee W: **AmpliSeq transcriptome analysis of human**
688 **alveolar and monocyte-derived macrophages over time in response to *Mycobacterium***
689 ***tuberculosis* infection.** *PLoS ONE* 2018, **13:**e0198221.

690 27. Jensen K, Gallagher IJ, Johnston N, Welsh M, Skuce R, Williams JL, Glass EJ:
691 **Variation in the early host-pathogen interaction of bovine macrophages with divergent**
692 ***Mycobacterium bovis* strains in the United Kingdom.** *Infect Immun* 2018, **86**.

693 28. Malone KM, Rue-Albrecht K, Magee DA, Conlon K, Schubert OT, Nalpas NC,
694 Browne JA, Smyth A, Gormley E, Aebersold R, et al: **Comparative 'omics analyses**
695 **differentiate *Mycobacterium tuberculosis* and *Mycobacterium bovis* and reveal distinct**
696 **macrophage responses to infection with the human and bovine tubercle bacilli.** *Microb*
697 *Genom* 2018**:**[Epub ahead of print].

698 29. Nalpas NC, Magee DA, Conlon KM, Browne JA, Healy C, McLoughlin KE, Rue-
699 Albrecht K, McGettigan PA, Killick KE, Gormley E, et al: **RNA sequencing provides**
700 **exquisite insight into the manipulation of the alveolar macrophage by tubercle bacilli.**
701 *Sci Rep* 2015, **5:**13629.

702 30. Lavalett L, Rodriguez H, Ortega H, Sadee W, Schlesinger LS, Barrera LF: **Alveolar**
703 **macrophages from tuberculosis patients display an altered inflammatory gene**
704 **expression profile.** *Tuberculosis* 2017, **107:**156-167.

705 31. Vegh P, Magee DA, Nalpas NC, Bryan K, McCabe MS, Browne JA, Conlon KM,
706 Gordon SV, Bradley DG, MacHugh DE, Lynn DJ: **MicroRNA profiling of the bovine**
707 **alveolar macrophage response to *Mycobacterium bovis* infection suggests pathogen**
708 **survival is enhanced by microRNA regulation of endocytosis and lysosome trafficking.**
709 *Tuberculosis* 2015, **95:**60-67.

710 32. Bierne H, Hamon M, Cossart P: **Epigenetics and bacterial infections.** *Cold Spring*
711 *Harb Perspect Med* 2012, **2:**a010272.

712 33. Hamon MA, Cossart P: **Histone modifications and chromatin remodeling during**
713 **bacterial infections.** *Cell Host Microbe* 2008, **4:**100-109.

714 34. Niller HH, Minarovits J: **Patho-epigenetics of infectious diseases caused by**
715 **intracellular bacteria.** *Adv Exp Med Biol* 2016, **879:**107-130.

716 35. Rolando M, Gomez-Valero L, Buchrieser C: **Bacterial remodelling of the host**
717 **epigenome: functional role and evolution of effectors methylating host histones.** *Cell*
718 *Microbiol* 2015, **17:**1098-1107.

719 36. Marr AK, MacIsaac JL, Jiang R, Airo AM, Kobor MS, McMaster WR: ***Leishmania***
720 ***donovani* infection causes distinct epigenetic DNA methylation changes in host**
721 **macrophages.** *PLoS Pathog* 2014, **10:**e1004419.

722 37. Zheng L, Leung ETY, Wong HK, Lui G, Lee N, To K-F, Choy KW, Chan RCY, Ip
723 M: **Unraveling methylation changes of host macrophages in *Mycobacterium tuberculosis***
724 **infection.** *Tuberculosis* 2016, **98:**139-148.

725 38. Sharma G, Sowpati DT, Singh P, Khan MZ, Ganji R, Upadhyay S, Banerjee S,
726 Nandicoori VK, Khosla S: **Genome-wide non-CpG methylation of the host genome**
727 **during *M. tuberculosis* infection.** *Sci Rep* 2016, **6:**25006.

728 39. Pennini ME, Perrinet S, Dautry-Varsat A, Subtil A: **Histone methylation by NUE, a**
729 **novel nuclear effector of the intracellular pathogen *Chlamydia trachomatis*.** *PLoS Pathog*
730 2010, **6:**e1000995.

731 40. Rolando M, Sanulli S, Rusniok C, Gomez-Valero L, Bertholet C, Sahr T, Margueron
732 R, Buchrieser C: ***Legionella pneumophila* effector RomA uniquely modifies host**
733 **chromatin to repress gene expression and promote intracellular bacterial replication.**
734 *Cell Host Microbe* 2013, **13:**395-405.

735 41. Yaseen I, Kaur P, Nandicoori VK, Khosla S: **Mycobacteria modulate host**
736 **epigenetic machinery by Rv1988 methylation of a non-tail arginine of histone H3.** *Nat*
737 *Commun* 2015, **6:**8922.

738 42. Bouttier M, Laperriere D, Memari B, Mangiapane J, Fiore A, Mitchell E, Verway M,
739 Behr MA, Sladek R, Barreiro LB, et al: **Alu repeats as transcriptional regulatory**
740 **platforms in macrophage responses to *M. tuberculosis* infection.** *Nucleic Acids Res* 2016,
741 **44:**10571-10587.

742 43. Arts RJW, Moorlag S, Novakovic B, Li Y, Wang SY, Oosting M, Kumar V, Xavier
743 RJ, Wijmenga C, Joosten LAB, et al: **BCG vaccination protects against experimental viral**
744 **infection in humans through the induction of cytokines associated with trained**
745 **immunity.** *Cell Host Microbe* 2018, **23:**89-100 e105.

746 44. Sims RJ, 3rd, Nishioka K, Reinberg D: **Histone lysine methylation: a signature for**
747 **chromatin function.** *Trends Genet* 2003, **19:**629-639.

748 45. Landt SG, Marinov GK, Kundaje A, Kheradpour P, Pauli F, Batzoglou S, Bernstein
749 BE, Bickel P, Brown JB, Cayting P, et al: **ChIP-seq guidelines and practices of the**
750 **ENCODE and modENCODE consortia.** *Genome Res* 2012, **22:**1813-1831.

751 46. Clouaire T, Webb S, Skene P, Illingworth R, Kerr A, Andrews R, Lee JH, Skalnik D,
752 Bird A: **Cfp1 integrates both CpG content and gene activity for accurate H3K4me3**
753 **deposition in embryonic stem cells.** *Genes Dev* 2012, **26:**1714-1728.

754 47. Barski A, Cuddapah S, Kartashov AV, Liu C, Imamichi H, Yang W, Peng W, Lane
755 HC, Zhao K: **Rapid recall ability of memory T cells is encoded in their epigenome.** *Sci*
756 *Rep* 2017, **7:**39785.

757 48. Vegh P, Foroushani AB, Magee DA, McCabe MS, Browne JA, Nalpas NC, Conlon
758 KM, Gordon SV, Bradley DG, MacHugh DE, Lynn DJ: **Profiling microRNA expression in**
759 **bovine alveolar macrophages using RNA-seq.** *Vet Immunol Immunopathol* 2013, **155:**238-
760 244.

761 49. Kramer A, Green J, Pollard J, Jr., Tugendreich S: **Causal analysis approaches in**
762 **Ingenuity Pathway Analysis.** *Bioinformatics* 2014, **30:**523-530.

763 50. Thomas PD, Campbell MJ, Kejariwal A, Mi H, Karlak B, Daverman R, Diemer K,
764 Muruganujan A, Narechania A: **PANTHER: a library of protein families and subfamilies**
765 **indexed by function.** *Genome Res* 2003, **13:**2129-2141.

766 51. Huang da W, Sherman BT, Lempicki RA: **Systematic and integrative analysis of**
767 **large gene lists using DAVID bioinformatics resources.** *Nat Protoc* 2009, **4:**44-57.

768 52. Richardson IW, Berry DP, Wiencko HL, Higgins IM, More SJ, McClure J, Lynn DJ,
769 Bradley DG: **A genome-wide association study for genetic susceptibility to**
770 ***Mycobacterium bovis* infection in dairy cattle identifies a susceptibility QTL on**
771 **chromosome 23.** *Genet Sel Evol* 2016, **48:**19.

772 53. Alcaraz-Lopez OA, Garcia-Gil C, Morales-Martinez C, Lopez-Rincon G, Estrada-
773 Chavez C, Gutierrez-Pabello JA, Esquivel-Solis H: **Divergent macrophage responses to**
774 ***Mycobacterium bovis* among naturally exposed uninfected and infected cattle.** *Immunol*
775 *Cell Biol* 2017, **95:**436-442.

776 54. Cheng J, Blum R, Bowman C, Hu D, Shilatifard A, Shen S, Dynlacht BD: **A role for**
777 **H3K4 monomethylation in gene repression and partitioning of chromatin readers.** *Mol*
778 *Cell* 2014, **53:**979-992.

779 55. LaMere SA, Thompson RC, Komori HK, Mark A, Salomon DR: **Promoter H3K4**
780 **methylation dynamically reinforces activation-induced pathways in human CD4 T cells.**
781 *Genes Immun* 2016, **17:**283-297.

782 56. Rawlings JS, Rosler KM, Harrison DA: **The JAK/STAT signaling pathway.** *J Cell*
783 *Sci* 2004, **117:**1281-1283.

784 57. Manca C, Tsenova L, Freeman S, Barczak AK, Tovey M, Murray PJ, Barry C,
785 Kaplan G: **Hypervirulent *M. tuberculosis* W/Beijing strains upregulate type I IFNs and**
786 **increase expression of negative regulators of the Jak-Stat pathway.** *J Interferon Cytokine*
787 *Res* 2005, **25:**694-701.

788 58. Cliff JM, Kaufmann SH, McShane H, van Helden P, O'Garra A: **The human**
789 **immune response to tuberculosis and its treatment: a view from the blood.** *Immunol Rev*
790 2015, **264:**88-102.

791 59. Pastuschek J, Poetzsch J, Morales-Prieto DM, Schleussner E, Markert UR, Georgiev
792 G: **Stimulation of the JAK/STAT pathway by LIF and OSM in the human granulosa**
793 **cell line COV434.** *J Reprod Immunol* 2015, **108:**48-55.

794 60. Marino VJ, Roguin LP: **The granulocyte colony stimulating factor (G-CSF)**
795 **activates Jak/STAT and MAPK pathways in a trophoblastic cell line.** *J Cell Biochem*
796 2008, **103:**1512-1523.

797 61. Polena H, Boudou F, Tilleul S, Dubois-Colas N, Lecointe C, Rakotosamimanana N,
798 Pelizzola M, Andriamandimby SF, Raharimanga V, Charles P, et al: ***Mycobacterium***
799 ***tuberculosis* exploits the formation of new blood vessels for its dissemination.** *Sci Rep*
800 2016, **6:**33162.

801 62. O'Kane CM, Elkington PT, Friedland JS: **Monocyte-dependent oncostatin M and**
802 **TNF-alpha synergize to stimulate unopposed matrix metalloproteinase-1/3 secretion**
803 **from human lung fibroblasts in tuberculosis.** *Eur J Immunol* 2008, **38:**1321-1330.

804 63. Martins A, Han J, Kim SO: **The multifaceted effects of granulocyte colony-**
805 **stimulating factor in immunomodulation and potential roles in intestinal immune**
806 **homeostasis.** *IUBMB Life* 2010, **62:**611-617.

807 64. Tsumura M, Okada S, Sakai H, Yasunaga S, Ohtsubo M, Murata T, Obata H, Yasumi
808 T, Kong XF, Abhyankar A, et al: **Dominant-negative STAT1 SH2 domain mutations in**
809 **unrelated patients with Mendelian susceptibility to mycobacterial disease.** *Hum Mutat*
810 2012, **33:**1377-1387.

811 65. Yu JS, Cui W: **Proliferation, survival and metabolism: the role of**
812 **PI3K/AKT/mTOR signalling in pluripotency and cell fate determination.** *Development*
813 2016, **143:**3050-3060.

814 66. Weichhart T, Saemann MD: **The PI3K/Akt/mTOR pathway in innate immune**
815 **cells: emerging therapeutic applications.** *Ann Rheum Dis* 2008, **67 Suppl 3:**iii70-74.

816 67. Yip SC, El-Sibai M, Coniglio SJ, Mouneimne G, Eddy RJ, Drees BE, Neilsen PO,
817 Goswami S, Symons M, Condeelis JS, Backer JM: **The distinct roles of Ras and Rac in PI**
818 **3-kinase-dependent protrusion during EGF-stimulated cell migration.** *J Cell Sci* 2007,
819 **120:**3138-3146.

820 68. Loo YM, Gale M, Jr.: **Immune signaling by RIG-I-like receptors.** *Immunity* 2011,
821 **34:**680-692.

822 69. Charrel-Dennis M, Latz E, Halmen KA, Trieu-Cuot P, Fitzgerald KA, Kasper DL,
823 Golenbock DT: **TLR-independent type I interferon induction in response to an**
824 **extracellular bacterial pathogen via intracellular recognition of its DNA.** *Cell Host*
825 *Microbe* 2008, **4:**543-554.

826 70. Dixit E, Kagan JC: **Intracellular pathogen detection by RIG-I-like receptors.** *Adv*
827 *Immunol* 2013, **117:**99-125.

828 71. Boxx GM, Cheng G: **The roles of type I interferon in bacterial infection.** *Cell Host*
829 *Microbe* 2016, **19:**760-769.

830 72. Mancuso G, Midiri A, Biondo C, Beninati C, Zummo S, Galbo R, Tomasello F,
831 Gambuzza M, Macri G, Ruggeri A, et al: **Type I IFN signaling is crucial for host**
832 **resistance against different species of pathogenic bacteria.** *J Immunol* 2007, **178:**3126-
833 3133.

834 73. O'Connell RM, Saha SK, Vaidya SA, Bruhn KW, Miranda GA, Zarnegar B, Perry
835 AK, Nguyen BO, Lane TF, Taniguchi T, et al: **Type I interferon production enhances**
836 **susceptibility to *Listeria monocytogenes* infection.** *J Exp Med* 2004, **200:**437-445.

837 74. Berry MP, Graham CM, McNab FW, Xu Z, Bloch SA, Oni T, Wilkinson KA,
838 Banchereau R, Skinner J, Wilkinson RJ, et al: **An interferon-inducible neutrophil-driven**
839 **blood transcriptional signature in human tuberculosis.** *Nature* 2010, **466:**973-977.

840 75. Mayer-Barber KD, Andrade BB, Oland SD, Amaral EP, Barber DL, Gonzales J,
841 Derrick SC, Shi R, Kumar NP, Wei W, et al: **Host-directed therapy of tuberculosis based**
842 **on interleukin-1 and type I interferon crosstalk.** *Nature* 2014, **511:**99-103.

843 76. Manca C, Tsenova L, Bergtold A, Freeman S, Tovey M, Musser JM, Barry CE, 3rd,
844 Freedman VH, Kaplan G: **Virulence of a *Mycobacterium tuberculosis* clinical isolate in**
845 **mice is determined by failure to induce Th1 type immunity and is associated with**
846 **induction of IFN-alpha /beta.** *Proc Natl Acad Sci U S A* 2001, **98:**5752-5757.

847 77. Nepal RM, Mampe S, Shaffer B, Erickson AH, Bryant P: **Cathepsin L maturation**
848 **and activity is impaired in macrophages harboring *M. avium* and *M. tuberculosis*.** *Int*
849 *Immunol* 2006, **18:**931-939.

850 78. Meenu S, Thiagarajan S, Ramalingam S, Michael A, Ramalingam S: **Modulation of**
851 **host ubiquitin system genes in human endometrial cell line infected with *Mycobacterium***
852 ***tuberculosis*.** *Med Microbiol Immunol (Berl)* 2016, **205:**163-171.

853 79. Silver RF, Walrath J, Lee H, Jacobson BA, Horton H, Bowman MR, Nocka K, Sypek
854 JP: **Human alveolar macrophage gene responses to *Mycobacterium tuberculosis* strains**
855 **H37Ra and H37Rv.** *Am J Respir Cell Mol Biol* 2009, **40:**491-504.

856 80. Hardbower DM, Asim M, Murray-Stewart T, Casero RA, Jr., Verriere T, Lewis ND,
857 Chaturvedi R, Piazuelo MB, Wilson KT: **Arginase 2 deletion leads to enhanced M1**
858 **macrophage activation and upregulated polyamine metabolism in response to**
859 ***Helicobacter pylori* infection.** *Amino Acids* 2016, **48:**2375-2388.

860 81. Lewis ND, Asim M, Barry DP, de Sablet T, Singh K, Piazuelo MB, Gobert AP,
861 Chaturvedi R, Wilson KT: **Immune evasion by *Helicobacter pylori* is mediated by**
862 **induction of macrophage arginase II.** *J Immunol* 2011, **186:**3632-3641.

863 82. Huang Z, Luo Q, Guo Y, Chen J, Xiong G, Peng Y, Ye J, Li J: ***Mycobacterium***
864 ***tuberculosis*-induced polarization of human macrophage orchestrates the formation and**
865 **development of tuberculous granulomas in vitro.** *PLoS ONE* 2015, **10:**e0129744.

866 83. Vogler M: **BCL2A1: the underdog in the BCL2 family.** *Cell Death Differ* 2012,
867 **19:**67-74.

868 84. Manzanillo PS, Shiloh MU, Portnoy DA, Cox JS: ***Mycobacterium tuberculosis***
869 **activates the DNA-dependent cytosolic surveillance pathway within macrophages.** *Cell*
870 *Host Microbe* 2012, **11:**469-480.

871 85. McNab F, Mayer-Barber K, Sher A, Wack A, O'Garra A: **Type I interferons in**
872 **infectious disease.** *Nat Rev Immunol* 2015, **15:**87-103.

873 86. Woo V, Alenghat T: **Host-microbiota interactions: epigenomic regulation.** *Curr*
874 *Opin Immunol* 2017, **44:**52-60.

875 87. Silmon de Monerri NC, Kim K: **Pathogens hijack the epigenome: a new twist on**
876 **host-pathogen interactions.** *Am J Pathol* 2014, **184:**897-911.

877 88. Sharma G, Upadhyay S, Srilalitha M, Nandicoori VK, Khosla S: **The interaction of**
878 **mycobacterial protein Rv2966c with host chromatin is mediated through non-CpG**
879 **methylation and histone H3/H4 binding.** *Nucleic Acids Res* 2015, **43:**3922-3937.

880 89. Magee DA, Conlon KM, Nalpas NC, Browne JA, Pirson C, Healy C, McLoughlin
881 KE, Chen J, Vordermeier HM, Gormley E, et al: **Innate cytokine profiling of bovine**
882 **alveolar macrophages reveals commonalities and divergence in the response to**
883 ***Mycobacterium bovis* and *Mycobacterium tuberculosis* infection.** *Tuberculosis (Edinb)*
884 2014, **94:**441-450.

885 90. Vernimmen D, Lynch MD, De Gobbi M, Garrick D, Sharpe JA, Sloane-Stanley JA,
886 Smith AJ, Higgs DR: **Polycomb eviction as a new distant enhancer function.** *Genes Dev*
887 2011, **25:**1583-1588.

888 91. O'Doherty AM, O'Shea LC, Fair T: **Bovine DNA methylation imprints are**
889 **established in an oocyte size-specific manner, which are coordinated with the expression**
890 **of the DNMT3 family proteins.** *Biol Reprod* 2012, **86:**67.

891 92. Andrews S: **FastQC: a quality control tool for high throughput sequence data.**
892 Babraham Research Campus, Cambridge, UK: Bioinformatics Group, Babraham Institute;
893 2016.

894 93. Martin M: **Cutadapt removes adapter sequences from high-throughput**
895 **sequencing reads.** *2011* 2011, **17:**3.

896 94. Lerdrup M, Johansen JV, Agrawal-Singh S, Hansen K: **An interactive environment**
897 **for agile analysis and visualization of ChIP-sequencing data.** *Nat Struct Mol Biol* 2016,
898 **23:**349-357.

899 95. Langmead B, Salzberg SL: **Fast gapped-read alignment with Bowtie 2.** *Nat*
900 *Methods* 2012, **9:**357-359.

901 96. Li H, Handsaker B, Wysoker A, Fennell T, Ruan J, Homer N, Marth G, Abecasis G,
902 Durbin R, Genome Project Data Processing S: **The Sequence Alignment/Map format and**
903 **SAMtools.** *Bioinformatics* 2009, **25:**2078-2079.

904 97. Feng J, Liu T, Zhang Y: **Using MACS to identify peaks from ChIP-Seq data.** *Curr*
905 *Protoc Bioinformatics* 2011, **Chapter 2:**Unit 2 14.

906 98. Thorvaldsdottir H, Robinson JT, Mesirov JP: **Integrative Genomics Viewer (IGV):**
907 **high-performance genomics data visualization and exploration.** *Brief Bioinform* 2013,
908 **14:**178-192.

909 99. Wilbanks EG, Facciotti MT: **Evaluation of algorithm performance in ChIP-seq**
910 **peak detection.** *PLoS ONE* 2010, **5:**e11471.

911 100. Stark R, Brown G: **DiffBind: differential binding analysis of ChIP-Seq peak data.**
912 **http://bioconductor.org/packages/release/bioc/vignettes/DiffBind/inst/doc/DiffBind.pdf.**
913 2011.

914 101. Patro R, Duggal G, Love MI, Irizarry RA, Kingsford C: **Salmon provides fast and**
915 **bias-aware quantification of transcript expression.** *Nat Methods* 2017, **14:**417-419.

916 102. Soneson C, Love MI, Robinson MD: **Differential analyses for RNA-seq:**
917 **transcript-level estimates improve gene-level inferences.** *F1000Res* 2015, **4:**1521.

918 103. Love MI, Huber W, Anders S: **Moderated estimation of fold change and**
919 **dispersion for RNA-seq data with DESeq2.** *Genome Biol* 2014, **15:**550.

920 104. Benjamini Y, Hochberg Y: **Controlling the false discovery rate - a practical and**
921 **powerful approach to multiple testing.** *J R Stat Soc Ser B Method* 1995, **57:**289-300.

922 105. Vejnar CE, Zdobnov EM: **MiRmap: comprehensive prediction of microRNA**
923 **target repression strength.** *Nucleic Acids Res* 2012, **40:**11673-11683.

924 106. Mi H, Huang X, Muruganujan A, Tang H, Mills C, Kang D, Thomas PD: **PANTHER**
925 **version 11: expanded annotation data from Gene Ontology and Reactome pathways,**
926 **and data analysis tool enhancements.** *Nucleic Acids Res* 2017, **45:**D183-D189.

927 107. Stelzer G, Rosen N, Plaschkes I, Zimmerman S, Twik M, Fishilevich S, Stein TI,
928 Nudel R, Lieder I, Mazor Y, et al: **The GeneCards Suite: from gene data mining to**
929 **disease genome sequence analyses.** *Curr Protoc Bioinformatics* 2016, **54:**1.30.31-31.30.33.

930
931

Figure 1

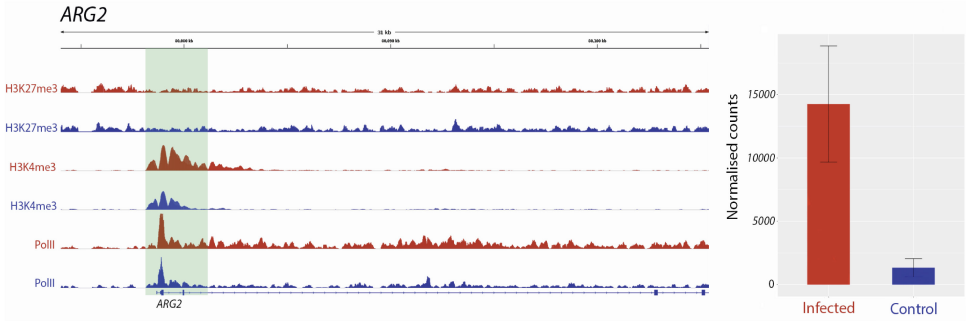
ARG2
H3K27me3
H3K27me3
H3K4me3
H3K4me3
PolII
PolII
ARG2
Normalised counts
15000
10000
5000
0
Infected
Control

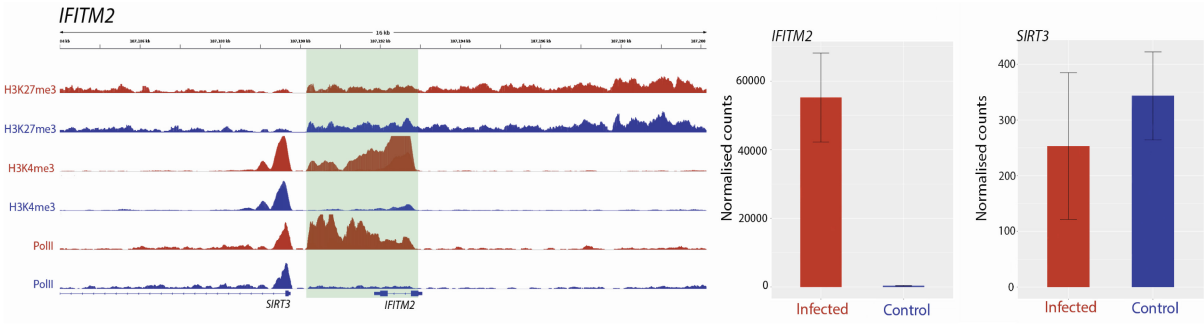
IFITM2
H3K27me3
H3K27me3
H3K4me3
H3K4me3
PolII
PolII
SIRT3
IFITM2
IFITM2
Normalised counts
60000
40000
20000
0
Infected
Control
SIRT3
Normalised counts
400
300
200
100
0
Infected
Control

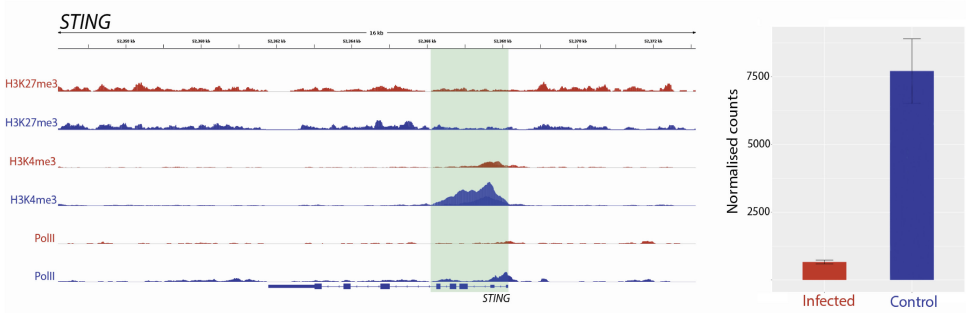
STING
H3K27me3
H3K27me3
H3K4me3
H3K4me3
PolII
PolII
STING
Normalised counts
7500
5000
2500
Infected
Control

Figure 2

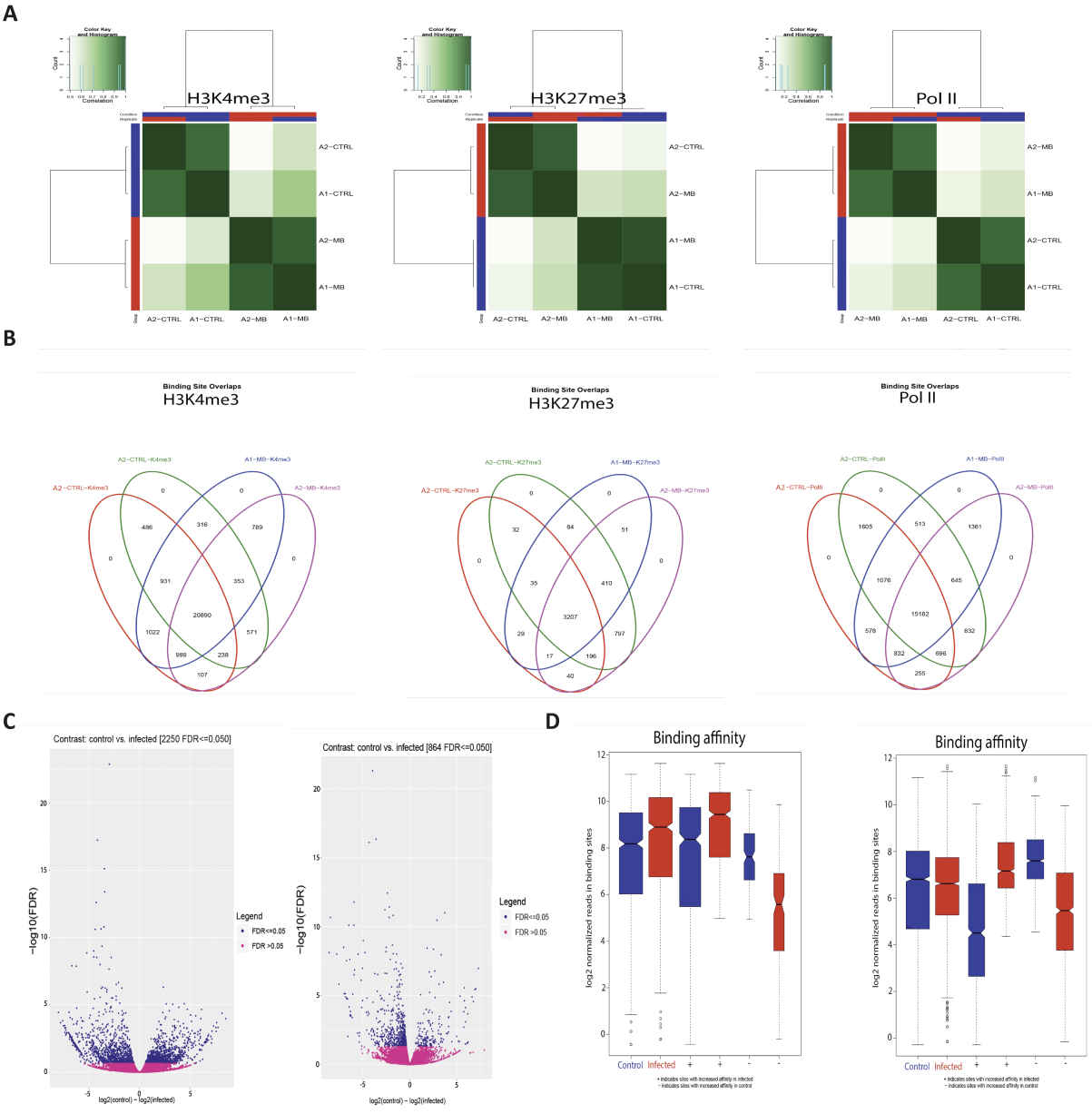
A
H3K4me3
H3K27me3
Pol II
Color Key and Histogram
Count
Correlation
A2−CTRL
A1−CTRL
A2−MB
A1−MB
B
Binding Site Overlaps
H3K4me3
H3K27me3
Pol II
A2−CTRL−K4me3
A1−MB−K4me3
A2−MB−K4me3
A2−CTRL−K27me3
A1−MB−K27me3
A2−MB−K27me3
A2−CTRL−PolII
A1−MB−PolII
A2−MB−PolII
C
Contrast: control vs. infected [2250 FDR<=0.050]
Contrast: control vs. infected [864 FDR<=0.050]
−log10(FDR)
log2(control) − log2(infected)
Legend
FDR<=0.05
FDR >0.05
D
Binding affinity
log2 normalized reads in binding sites
Control
Infected

938 **Figure 3**

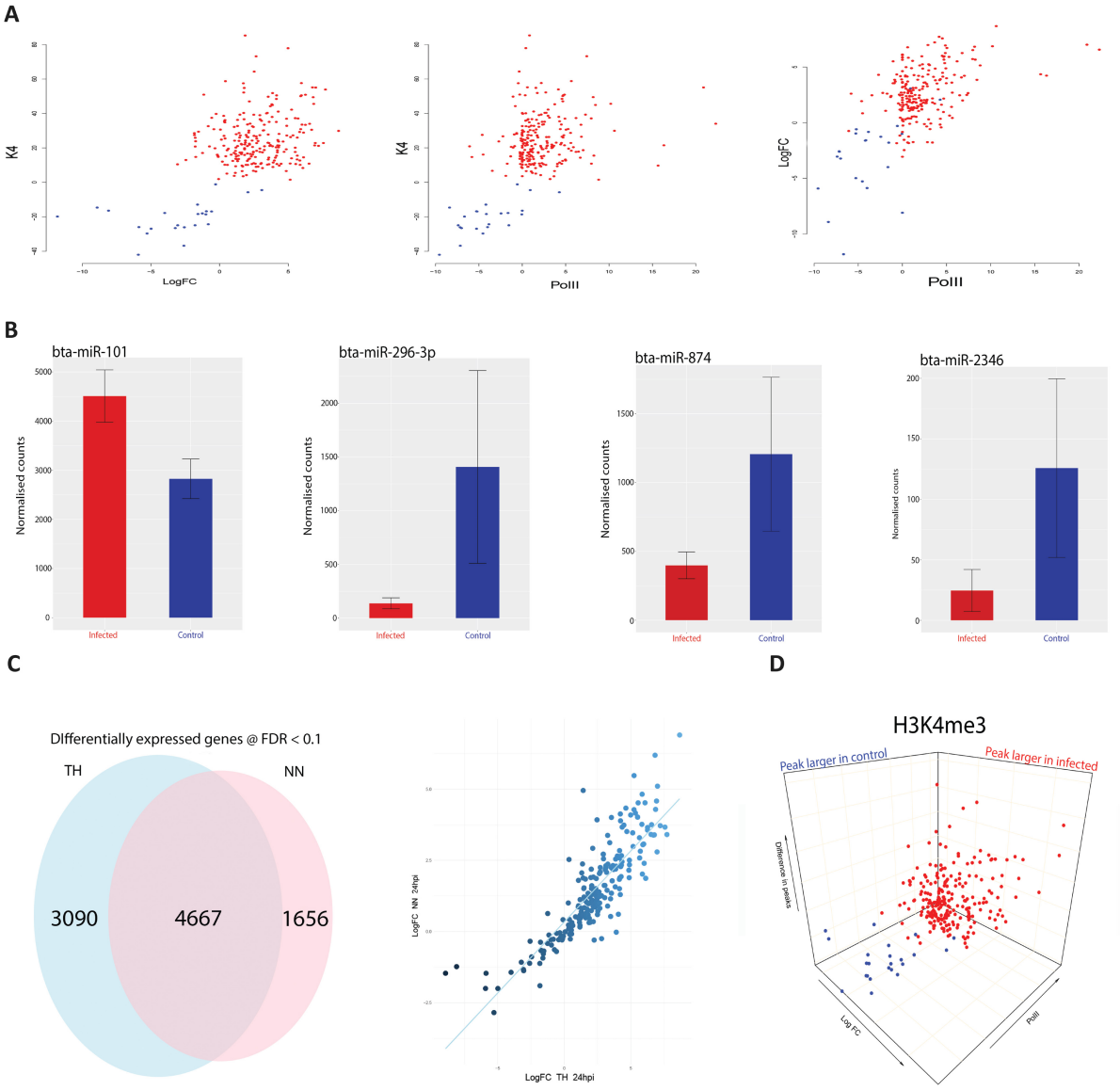

939

940

Figure 4

A

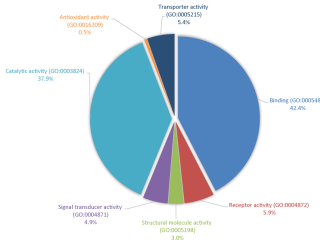

Molecular function

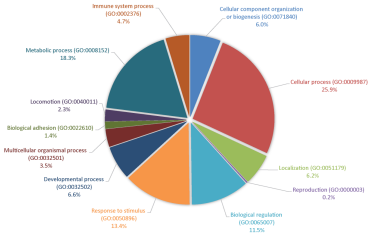

Biological process

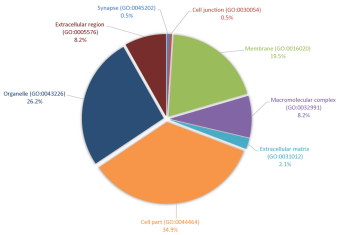

Cellular component

B

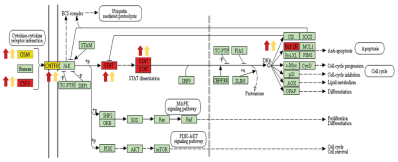

JAK-STAT signalling pathway

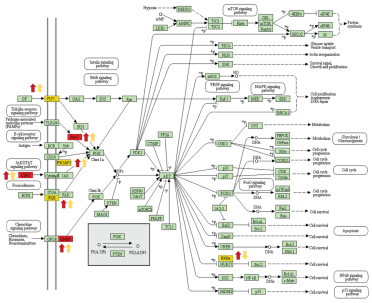

PI3-AKT signalling pathway

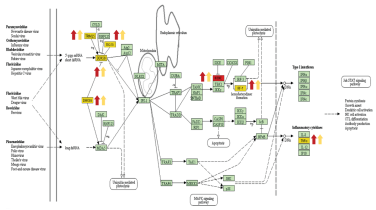

RIG-I-like signalling pathway

C

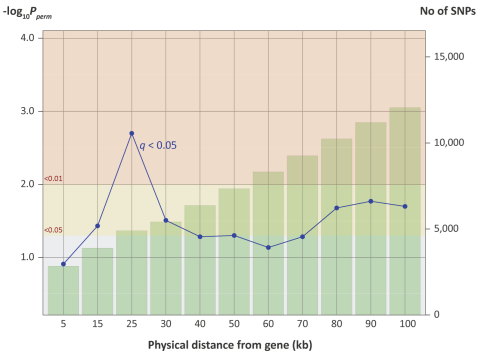

D

SNP	Gene	Function
rs109467646	*ABTB2*	Protein heterodimerization activity
rs42340336	*ARID5B*	RNA polymerase II regulatory region sequence-specific DNA binding
rs43291594	*CLMP*	Cell-cell adhesion
rs43291608	*CLMP*	Cell-cell adhesion
rs43291613	*CLMP*	Cell-cell adhesion
rs135643197	*CLMP*	Cell-cell adhesion
rs43291628	*CLMP*	Cell-cell adhesion
rs43292253	*CLMP*	Cell-cell adhesion
rs43292266	*CLMP*	Cell-cell adhesion
rs43292281	*CLMP*	Cell-cell adhesion
rs43292303	*CLMP*	Cell-cell adhesion
rs43292326	*CLMP*	Cell-cell adhesion
rs43293441	*CLMP*	Cell-cell adhesion
rs29014510	*CLMP*	Cell-cell adhesion
rs134561028	*CTSL*	Histone binding
rs42247932	*CTSL*	Histone binding
rs110265685	*EDN1*	Regulation of endothelin secretion
rs133489745	*MIC1*	MICOS complex
rs135121106	*RNFT1*	Integral component of membrane
rs133286573	*SAMSN1*	Phosphotyrosine residue binding
rs134127062	*TNFAIP3*	Ligase activity
rs137535115	*TNFAIP3*	Ligase activity